Journal of King Saud University – Science 34 (2022) 102155

Contents lists available at ScienceDirect

Journal of King Saud University – Science

journal homepage: www.sciencedirect.com

Original article

Exploring the phytochemicals of *Platycodon grandiflorus* for TMPRSS2 inhibition in the search for SARS-CoV-2 entry inhibitors

Arun Bahadur Gurung [a,*], Mohammad Ajmal Ali [b], Joongku Lee [c], Reem M. Aljowaie [b], Saeedah M. Almutairi [b]

[a] Department of Basic Sciences and Social Sciences, North-Eastern Hill University, Shillong 793022, Meghalaya, India
[b] Department of Botany and Microbiology, College of Science, King Saud University, P.O. Box 2455, Riyadh 11451, Saudi Arabia
[c] Department of Environment and Forest Resources, Chungnam National University, 99 Daehak-ro, Yuseong-gu, Daejeon 34134, Republic of Korea

ARTICLE INFO

Article history:
Received 26 January 2022
Revised 29 May 2022
Accepted 2 June 2022
Available online 9 June 2022

Keywords:
TMPRSS2
SARS-CoV-2
COVID-19
Platycodon grandiflorus
Molecular docking
Phytochemicals
Bioactive compounds

ABSTRACT

Platycodon grandiflorus (Jacq.) A. DC. (Campanulaceae) is commonly known as a balloon flower whose rhizomes have been widely utilized in traditional Chinese medicine (TCM) and in various Japanese prescriptions for the treatment of respiratory diseases, diabetes, and inflammatory disorders. The severe acute respiratory syndrome coronavirus 2 (SARS-CoV-2), the causative agent of coronavirus disease 2019 (COVID-19) global pandemic requires priming of the virus's spike (S) protein by cleavage of the S proteins by a multi-domain type II transmembrane serine protease, transmembrane protease serine 2 (TMPRSS2) to gain entry into the host cell. The current research aims at the screening of active phytocompounds of *P. grandiflorus* as potential inhibitors of cellular TMPRSS2 using molecular docking and molecular dynamics simulations approach. *In silico* toxicity analyses show that out of a total of 34 phytocompounds selected for the study, 12 compounds obey Lipinski's rule of five and have favourable pharmacokinetic properties. The top three lead molecules identified here were Apigenin, Luteolin and Ferulic acid which exhibited binding energies of −7.47 kcal/mol, −6.8 kcal/mol and −6.62 kcal/mol respectively with corresponding inhibition constants of 3.33 μM, 10.39 μM and 13.95 μM. The complexes between the lead molecules and the receptor were held by hydrogen bond interactions with key residues such as Gly383, Gly385, Glu389, Lys390, Asp435, Ser436, Ser441, Cys465 and Lys467, and hydrophobic interactions with surrounding residues. The stability of the protein–ligand complexes was evaluated during 100 ns molecular dynamics (MD) simulation by analysing key geometric properties such as RMSD, RMSF, radius of gyration, total solvent accessible surface area and the number of hydrogen bonds. The binding free energies analysis using MD simulations revealed that the compounds and TMPRSS2 have favourable thermodynamic interactions, which are primarily driven by van der Waals forces. As a result, the selected bioactive phytochemicals from *P. grandiflorus* that target the cellular TMPRSS2 could offer an alternative treatment option against SARS-CoV-2 infections.

1. Introduction

Platycodon grandiflorus (Jacq.) A. DC. is the only single species of the Platycodon genus, (Campanulaceae), commonly known as balloon flower. China, Korea, Japan, Mongolia, and Russia are all home to this species. *P. grandiflorus* is quite common in China, and its cultivation sites may be found throughout the country (Zhang et al., 2015). The rhizomes of *P. grandiflorus* are popularly known as *Jiegeng* or *Lingdanghua* in China, *Doraji* in North Korea, *Kikyo* in Japan, and *Huridunzhaga* in Mongolia (China Pharmacopoeia Committee, 2005). *P. grandiflorus* is a perennial plant that grows to a height of 20–120 cm. The leaves are green, ovate, elliptic, or lanceolate, and measure 2–7 0.5–3.5 cm^2. It has a blue or purple bloom that is 1.5–4.5 cm^2 in size. Because of its importance as traditional medicine and food resource, *P. grandiflorus* roots and rhizomes are usually collected around August (Huang, 2008). *P. grandiflorus* thrives in sunny herbal communities in thickets and is only seldom seen in woods below 2000 m in height, owing to its high ecological flexibility (Zhang et al., 2015). The rhizomes of *P. grandiflorus* have been widely utilized in traditional Chinese

* Corresponding author.
E-mail address: arunbgurung@gmail.com (A.B. Gurung).
Peer review under responsibility of King Saud University.

Production and hosting by Elsevier

https://doi.org/10.1016/j.jksus.2022.102155

medicine (TCM) with outstanding therapeutic benefits for the treatment of cough, excessive phlegm, and sore throat (China Pharmacopoeia Committee, 2005). Its rhizomes are traditionally used in various Japanese prescriptions to treat suppuration, chronic rhinitis, chronic tonsillitis, and other ailments (Zhang et al., 2015). The roots of *P. grandiflorus* were utilized to treat bronchitis, asthma, pulmonary tuberculosis (TB), diabetes, and inflammatory disorders in Korea after being grown for four years (Lee, 1973; Takagi and Lee, 1972). Furthermore, this plant may be utilized as a food source and is prepared into delectable meals in East Asian nations including China, Japan, and Korea (China Pharmacopoeia Committee, 2005).

The severe acute respiratory syndrome coronavirus 2 (SARS-CoV-2) depends on the host protein angiotensin-converting enzyme 2 (ACE2) receptor for entry into the host cells (Hoffmann et al., 2020). The viral entry necessitates not only binding to the ACE2 receptor but also priming of the virus's spike (S) protein by cleavage of the S proteins at the S1/S2 and S2 sites by a multidomain type II transmembrane serine protease, transmembrane protease serine 2 (TMPRSS2) (Baughn et al., 2020). This cleavage process is necessary for the virus to fuse with the host cell membrane and enter the cell (Hoffmann et al., 2020; Matsuyama et al., 2020). TMPRSS2 and ACE2 are co-expressed in several tissues such as the lung, heart, stomach, smooth muscle, liver, kidney, neurons, and immune cells (Fathema et al., 2021; Fuentes-Prior, 2021; Gemmati et al., 2020). Besides, both are abundantly present in type II pneumocyte cells (Kaur et al., 2021). Given the critical function of TMPRSS2 in viral entry and the lack of approved treatments for addressing the current coronavirus disease 2019 (COVID-19) pandemic, drug repurposing strategies to block this protease have received much consideration. Camostat, nafamostat, and gabexate, which are clinically authorized pharmacologic treatments of pancreatitis in Japan, can also suppress the activity of TMPRSS2 (Yamaya et al., 2020). Given the importance of host TMPRSS2 in the pathogenesis of SARS-CoV-2 infections, our current research focuses on the binding potential of a few selected active compounds of *Platycodon grandiflorus* to human TMPRSS2 using molecular docking, as well as probing the structural changes in the target protein induced by binding of the active compounds using molecular dynamics simulations approach. The phytochemicals proposed in the study are most likely to suppress TMPRSS2 function, preventing the SARS-CoV-2 virus from infecting host cells.

2. Materials and methods

2.1. Protein preparation

The three-dimensional structure of TMPRSS2 was obtained from the research collaboratory for structural bioinformatics (RCSB) protein data bank (PDB) using PDB ID: 7MEQ which was determined using the X-ray diffraction technique with a resolution of 1.95 Å. The hetero atoms-ions, water molecules and co-crystallized ligands were removed from the protein structure for docking studies and H-atoms were inserted using AutoDock Tools-1.5.6 (Morris et al., 2009).

2.2. Ligand preparation:

The information on thirty-four phytochemicals of *P. grandiflorus* was obtained through a literature search (Zhang et al., 2015). The structures of the phytochemicals along with Nafamostat (control) were retrieved from the PubChem database (Kim et al., 2016) and their structures were optimised using Merck molecular force field (MMFF)94 force field (Halgren, 1996).

2.3. Calculation of drug-like properties

The phytochemicals were evaluated for drug-likeness using Lipinski's rule of five (ROF) (Lipinski, 2004). The physicochemical properties of the compounds were determined using the DataWarrior tool version 4.6.1. (Sander et al., 2015).

2.4. Validation of the docking process

Initially, the docking procedure was validated by re-docking the co-crystal ligand of TMPRSS2, 4-carbamimidamidobenzoic acid (GBS). The re-docked ligand was used to evaluate if the root mean square deviation (RMSD) between the docked and native position is within $\leq$2.0 Å.

2.5. Molecular docking

Molecular docking studies were performed with TMPRSS2 protein and the active compounds of *P. grandiflorus* using the AutoDock 4.2 program (Morris et al., 2009). This docking program operates using a Lamarckian genetic algorithm (LGA) (Morris et al., 1998). The active sites were input and a grid parameter file for the protein was generated by fixing the number of grid points on the x, y, and z axes to 70 × 70 × 70 with a grid box centred

Table 1
List of bioactive compounds from *P. grandiflorus* selected for the *in silico* studies.

Compounds	Name	Class	PubChem CID
1	Platycodin A	Triterpenoid saponins	46173910
2	Platycodin C	Triterpenoid saponins	46173919
3	Platycodin D	Triterpenoid saponins	162859
4	Platycodin D2	Triterpenoid saponins	53317652
5	Deapioplatycodin D	Triterpenoid saponins	70698266
6	Platycodin D3	Triterpenoid saponins	70698293
7	Luteolin-7-O-glucoside	Flavonoids	5280637
8	Apigenin-7-O-glucoside	Flavonoids	5280704
9	Apigenin	Flavonoids	5280443
10	(2R,3R)-taxifolin	Flavonoids	439533
11	Luteolin	Flavonoids	5280445
12	Quercetin-7-O-glucoside	Flavonoids	5381351
13	Quercetin-7-O-rutinoside	Flavonoids	44259247
14	Platyconin	Flavonoids	90659256
15	Flavoplatycoside	Phenolic acids	10416329
16	Caffeic acid	Phenolic acids	689043
17	3,4-dimethoxycinnamic acid	Phenolic acids	717531
18	Ferulic acid	Phenolic acids	445858
19	Isoferulic acid	Phenolic acids	736186
20	*m*-coumaric acid	Phenolic acids	637541
21	*p*-coumaric acid	Phenolic acids	637542
22	*p*-hydroxybenzoic acid	Phenolic acids	135
23	α-resorcylic acid	Phenolic acids	528564
24	2,3-dihydroxybenzoic acid	Phenolic acids	19
25	2-hydroxy-4-methoxybenzoic acid	Phenolic acids	10210429
26	Homovanillic acid	Phenolic acids	1738
27	Chlorogenic acid	Phenolic acids	1794427
28	Lobetyolinin	Polyacetylene	5459227
29	Lobetyolin	Polyacetylene	6369123
30	Betulin	Sterols	72326
31	β-sitosterol	Sterols	222284
32	δ-7-stigmastenone-3	Sterols	5748344
33	Spinasterol	Sterols	5281331
34	α-spinasteryl-3-O-β-D-glucoside	Sterols	12960498

at x:-7.6961, y:-7.7232, z:18.3699 centred at the co-crystal ligand. AutoDock grids were calculated for regularly spaced points at intervals of 0.375 Å contained within a cube based on the active sites of TMPRSS2 protein. The population size was set to 250 and the individuals were initialized randomly. The maximum number of energy evaluations was set to 10^6, and the maximum number of generations was 1000. Other docking parameters were set to the default values. The Lamarckian genetic algorithm was chosen to determine the best conformers in fifty independent trials of each compound. The LigPlot$^+$ v.1.4.5 tool (Laskowski and Swindells, 2011) was used to study the molecular interactions between the compounds and the target protein.

2.6. Molecular dynamics simulation

The lead compounds discovered from the docking experiments, as well as the reference molecule, were submitted to Molecular Dynamics (MD) simulations to get a better understanding of the protein–ligand interactions. The PRODRG server (Schüttelkopf and Van Aalten, 2004) was used to build ligand topologies, whereas the Gromos96 43 B1 force field was used to generate protein topologies in Groningen Machine for Chemical Simulations (GROMACS) 5.0.6 (Hess et al., 2008). The three-site transferable intermolecular potential (SPC216) water model was used to solve a triclinic box, which was then neutralized with counterions. All of the problematic connections were eliminated further by running the system through a 10,000-step steepest descent algorithm with a force limit of <1000 kJ/mol (Bavi et al., 2016). Following that, the equilibration was carried out using the Number of particles, Volume and Temperature (NVT) (Berendsen et al., 1984) and Number of particles, Pressure and Temperature (NPT) (Parrinello and Rahman, 1981) methods at 100 ps at 300 K and 100 ps at a pressure of 1 bar maintained by a Parrinello-Rahman barostat and allowing the movement of counterions and water molecules while constraining the protein backbone. The long-range electrostatic interaction was computed using Particle Mesh Ewald (PME) (Darden et al., 1993), with a cut-off distance of 12 Å for Coulombic and van der Waals interactions. MD simulations were run for 100 ns, with coordinate data being saved every 2 fs. The Xmgrace plotting tool was used to analyze the corresponding findings.

2.7. MM/PBSA binding energy analysis

The binding free energy (ΔG_{bind}) of the compounds was determined using the LARMD program (Yang et al., 2020) which employs the equation below Eq. (1).

$$\Delta G_{bind} = \Delta E_{bind} - T\Delta S_{sol} - T\Delta S_{conf}$$

where ΔE_{bind} corresponds to the binding energy, $T\Delta S_{sol}$ is the solvation entropy and $T\Delta S_{conf}$ represents the conformational entropy. The enthalpy was calculated using the Molecular mechanics Poisson–Boltzmann surface area (MM-PBSA) or molecular mechanics generalised Born surface area (MM-GBSA) method (Hou et al., 2011), while the entropy was calculated using an empirical method (Hao et al., 2009; Pan et al., 2008).

3. Results:

We chose 34 major bioactive compounds discovered in *P. grandiflorus* extracts for this investigation which belong to different classes such as Triterpenoid saponins (Platycodin A, Platycodin C, Platycodin D, Platycodin D2, Deapioplatycodin D and Platycodin D3), Flavonoids (Luteolin-7-O-glucoside, Apigenin-7-O-glucoside, Apigenin, (2R,3R)-taxifolin, Luteolin, Quercetin-7-O-glucoside.

Table 2
Drug-like properties of the bioactive compounds from *P. grandiflorus* where the asterisk indicates compound obeying the Lipinski's rule of five criteria.

Compounds	Name	MW	cLogP	HBA	HBD	TPSA	RB
1	Platycodin A	1267.37	−3.5801	29	16	459.35	17
2	Platycodin C	1267.37	−3.5801	29	16	459.35	17
3	Platycodin D	1225.33	−4.0647	28	17	453.28	15
4	Platycodin D2	1387.47	−5.9018	33	20	532.43	18
5	Deapioplatycodin D	1093.21	−2.711	24	15	394.36	12
6	Platycodin D3	1387.47	−5.9018	33	20	532.43	18
7	Luteolin-7-O-glucoside	448.379	7.00E-04	11	7	186.37	4
8	Apigenin-7-O-glucoside	432.38	0.3464	10	6	166.14	4
9*	Apigenin	270.239	2.3357	5	3	86.99	1
10*	(2R,3R)-taxifolin	304.253	0.9579	7	5	127.45	1
11*	Luteolin	286.238	1.99	6	4	107.22	1
12	Quercetin-7-O-glucoside	464.378	−0.4991	12	8	206.6	4
13	Quercetin-7-O-rutinoside	610.519	−1.4095	16	10	265.52	6
14	Platyconin	1421.23	−4.9099	37	21	596.03	23
15	Flavoplatycoside	612.535	−1.9418	16	10	265.52	6
16*	Caffeic acid	180.159	0.7825	4	3	77.76	2
17*	3,4-dimethoxycinnamic acid	208.212	1.3339	4	1	55.76	4
18*	Ferulic acid	194.185	1.0582	4	2	66.76	3
19*	Isoferulic acid	194.185	1.0582	4	2	66.76	3
20*	*m*-coumaric acid	164.16	1.1282	3	2	57.53	2
21*	*p*-coumaric acid	164.16	1.1282	3	2	57.53	2
22*	*p*-hydroxybenzoic acid	138.122	0.799	3	2	57.53	1
23	α-resorcylic acid	496.91	9.314	4	0	44.76	10
24*	2,3-dihydroxybenzoic acid	154.121	0.4533	4	3	77.76	1
25	2-hydroxy-4-methoxybenzoic acid	583.719	3.9151	5	4	81.95	16
26*	Homovanillic acid	182.174	0.7271	4	2	66.76	3
27	Chlorogenic acid	354.31	−0.7685	9	6	164.75	5
28	Lobetyolinin	558.575	−2.5943	13	9	218.99	12
29	Lobetyolin	396.434	−0.7572	8	6	139.84	9
30	Betulin	442.725	6.7202	2	2	40.46	2
31	β-sitosterol	414.715	7.8552	1	1	20.23	6
32	δ-7-stigmastenone-3	412.699	7.9989	1	0	17.07	6
33	Spinasterol	412.699	7.603	1	1	20.23	5
34	α-spinasteryl-3-O-β-D-glucoside	574.84	5.7659	6	4	99.38	8

Quercetin-7-O-rutinoside, Platyconin), Phenolic acids (Flavoplatycoside, Caffeic acid, 3,4-dimethoxycinnamic acid, Ferulic acid, Isoferulic acid, *m*-coumaric acid, *p*-coumaric acid, *p*-hydroxybenzoic acid, α-resorcylic acid, 2,3-dihydroxybenzoic acid, 2-hydroxy-4-methoxybenzoic acid, Homovanillic acid, Chlorogenic acid), Polyacetylene (Lobetyolinin, Lobetyolin) and Sterols (Betulin, β-sitosterol, δ-7-stigmastenone-3, Spinasterol, α-spinasteryl-3-O-β-D-glucoside) (Table 1). These molecules were subjected to ROF filters (molecular mass <500 Da, hydrogen bond donors <5, hydrogen bond acceptors <10, and a log P octanol–water partition coefficient <5) yielding 12 orally bioactive compounds (Table 2). The chemical structures of the filtered compounds utilised for molecular docking studies are depicted in Fig. 1. A redocking experiment shows an RMSD value of 1.060 Å between the native and docked positions of the cocrystal ligand (Fig. 2). An RMSD value <2.0 Å suggests that molecular docking parameters used in the study can precisely predict the binding poses of the compounds. The molecular docking results of the filtered bioactive compounds of *P. grandiflorus* as well as the control (Nafamostat) against the target receptor TMPRSS2 are displayed in Table 3. Three compounds were shown to have the best docking with TMPRSS2: apigenin, luteolin, and ferulic acid. Apigenin binds to TMPRSS2 with a binding energy of −7.47 kcal/mol and inhibition constant of 3.33 μM forming four hydrogen bonds with Gly383, Gly385, Glu389 and Cys465 and hydrophobic interactions with Gly259, Trp384, Ala386, Thr387, Glu388, Asn398, Ala399, Ala400, Asp435, Cys437, Asp440 and Ala466 (Fig. 3A). Luteolin binds to TMPRSS2 with a binding energy of −6.8 kcal/mol and inhibition constant of 10.39 μM and establishes four hydrogen bonds with Lys390, Ser436 and Ser441 and hydrophobic interactions with Glu389, Asp435, Cys437, Gln438, Thr459, Ser460, Trp461, Gly464, Cys465 and Gly472 (Fig. 3B). Ferulic acid interacts with TMPRSS2 with a binding energy of −6.62 kcal/mol and inhibition constant of 13.95 μM and establishes four hydrogen bonds with Glu389, Asp435 and Lys467 as well as hydrophobic interactions with Ala386, Thr387, Glu388, Asn433, Ser436, Cys437, Asp440, Cys465 and Ala466 (Fig. 3C). The control drug, Nafamostat binds to TMPRSS2 with a binding energy of −9.19 kcal/mol and inhibition constant of 0.184 μM and establishes six hydrogen bonds with His296, Asp345 and Gly464 and hydrophobic interactions with Val280, Cys281, Cys297, Leu302, Asp435, Ser436, Cys437, Gln438, Ser441, Ser460, Trp461, Gly462 and Cys465 (Fig. 3D).

MD simulations of the unbound TMPRSS2 and its complexes with the top three ranking compounds-Apigenin, Luteolin, Ferulic acid, and the control (Nafamostat) were performed for 100 ns, and various geometrical properties were determined from their trajectories (Table S1). The root-mean-square deviation (RMSD) is a valuable metric for assessing the atomic position structural deviation and protein structural stability. The average RMSD of backbone atoms of TMPRSS2, TMPRSS2_Apigenin, TMPRSS2_Luteolin

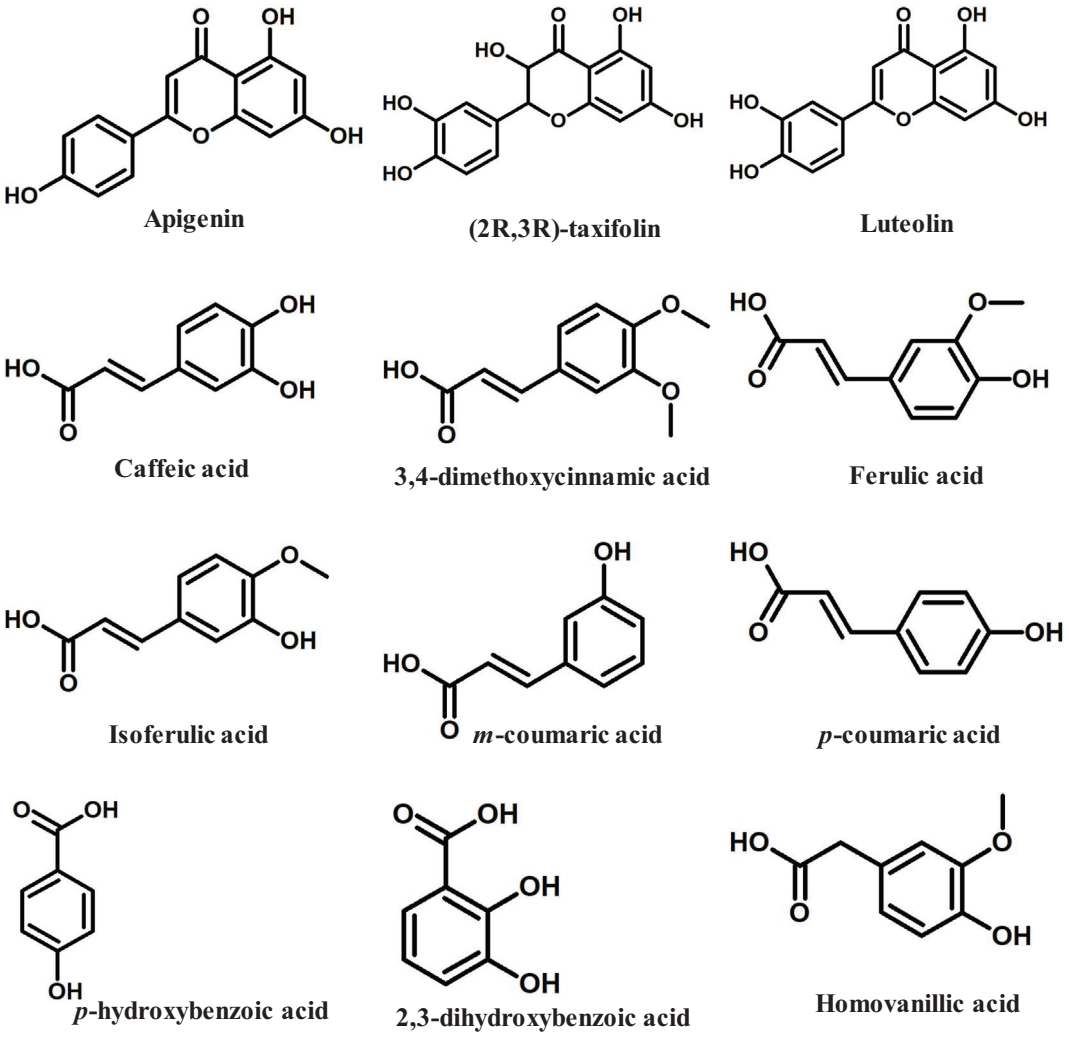

Fig. 1. The drug-like bioactive compounds from *P. grandiflorus* used for molecular docking experiment.

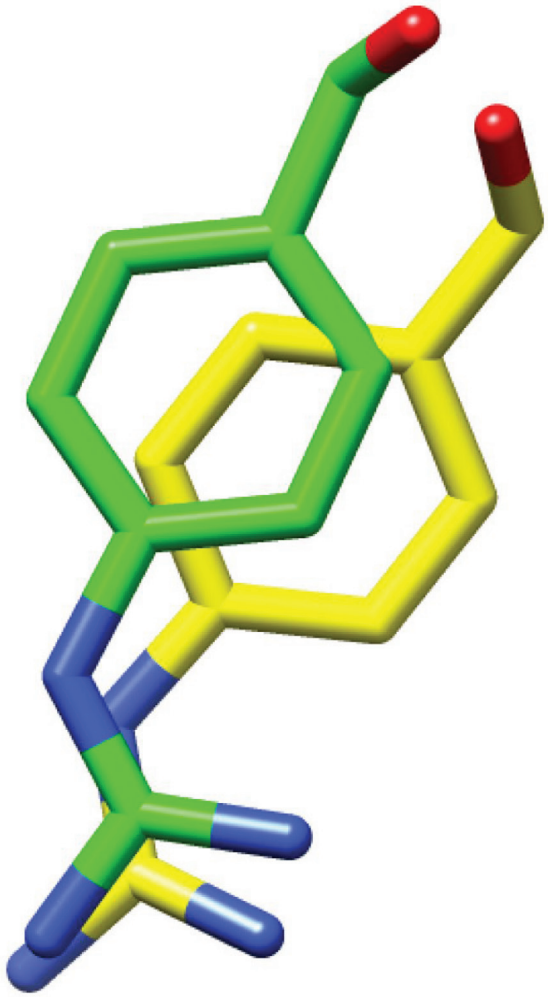

Fig. 2. Superposition of the native conformation (yellow) of the co-crystal ligand (GBS) with its docked pose (green) revealed an RMSD of 1.060 Å.

and TMPRSS2_Ferulic acid and TMPRSS2_Nafamostat complexes were 0.33161855 ± 0.020691134 nm, 0.282429554 ± 0.04350818 3 nm, 0.32489471 ± 0.045273601 nm, 0.304615439 ± 0.0320351 41 nm and 0.300230713 ± 0.028235882 nm respectively (Table S1). The binding of the compounds induces a reduction in the structural flexibility of the target enzyme (Fig. 4). The average RMSD values of Apigenin, Luteolin, Ferulic acid and the Nafamostat were 0.247362992 ± 0.062295857 nm, 0.576125057 ± 0.2147724 52 nm, 0.730537652 ± 0.21814513 nm and 0.507619867 ± 0.078 623572 nm indicating that the compounds have favourable binding orientations in the target enzyme's binding pocket. To analyse the local fluctuations in the target enzyme before and after compound binding, an average of the residual fluctuations in TMPRSS2 was computed and plotted as the root-mean-square fluctuation (RMSF) (Fig. 5). The RMSF figure revealed significant residual variations in several locations in the target enzyme, with high amplitudes of fluctuations in Ser204 (0.5562 nm), Gly205 (0.5075 nm), Gln253 (0.5027 nm), Ser254 (0.4391 nm), Arg255 (0.7522 nm), Ser339 (0.4562 nm), Lys340 (0.5289 nm), Glu388 (0.6266 nm),

Table 3
Molecular docking analysis of filtered compounds from *P. grandiflorus* and a control (Nafamostat).

Compounds	Name	Binding energy (kcal/mol)	Inhibition constant (μM)
9	Apigenin	−7.47	3.33
10	(2R,3R)-taxifolin	−6.34	22.67
11	Luteolin	−6.8	10.39
16	Caffeic acid	−6.38	21.13
17	3,4-dimethoxycinnamic acid	−6.41	19.91
18	Ferulic acid	−6.62	13.95
19	Isoferulic acid	−6.27	25.57
20	*m*-coumaric acid	−5.92	45.46
21	*p*-coumaric acid	−6.41	20.09
22	*p*-hydroxybenzoic acid	−3.94	1290
24	2,3-dihydroxybenzoic acid	−4.02	1130
26	Homovanillic acid	−4.61	419.57
	Nafamostat (Control)	−9.19	0.184

Glu389 (0.6227 nm) and Lys390 (0.6265 nm). The radius of gyration (Rg) of unbound TMPRSS2 and TMPRSS2 docked complexes were determined to measure their structural compactness (Fig. 6). The Rg values TMPRSS2, TMPRSS2_Apigenin, TMPRSS2_Luteolin and TMPRSS2_Ferulic acid and TMPRSS2_Nafamostat complexes were 2.072465355 ± 0.014329819 nm, 2.080123706 ± 0.012810064 nm, 2.06185013 ± 0.013976506 nm, 2.067286903 ± 0.020060061 nm and 2.074381249 ± 0.01411647 nm respectively. The TMPRSS2_Luteolin and TMPRSS2_Ferulic acid complexes show slightly lower Rg values whereas TMPRSS2_Apigenin and TMPRSS2_Nafamostat show higher Rg values when compared to unbound TMPRSS2. The Rg plot analysis, in this case, reveals that TMPRSS2 protein undergoes conformational changes in response to the binding of compounds, resulting in changes in structural compactness. The solvent-accessible surface area (SASA) of a protein is the part of the protein that interacts directly with the solvent molecules around it. The SASA plot for unbound TMPRSS2 and TMPRSS2 docked complexes was generated during the 100 ns MD simulation. (Fig. 7). The unbound TMPRSS2, TMPRSS2_Apigenin, TMPRSS2_Luteolin, TMPRSS2_Ferulic acid and TMPRSS2_Nafamostat complexes show average SASA values of 150.9597053 ± 3.249067344 nm^2, 152.919972 ± 2.82381675 nm^2, 152.9353017 ± 3.806978439 nm^2, 153.5488102 ± 5.332797744 nm^2 and 153.0 682637 ± 3.424944207 nm^2 respectively. A decrease in total SASA after interaction with the compounds was observed due to the conformational changes in the protein. Intramolecular hydrogen bonding plays a significant role in determining a protein's stability and overall structure. The stability of unbound TMPRSS2 and TMPRSS2 docked complexes was confirmed by monitoring hydrogen bonds established throughout the simulation (Fig. S1. A). The average number of intramolecular hydrogen bonds in TMPRSS2, TMPRSS2_Apigenin, TMPRSS2_Luteolin, TMPRSS2_Ferulic acid and TMPRSS2_Nafamostat complexes were 225.1298701 ± 9.051691382, 215.3916084 ± 8.497675536, 218.1968032 ± 8.978 431365, 225.8011988 ± 9.14677203, 223.5194805 ± 8.42637942 respectively. The compounds- Apigenin, Luteolin, Ferulic acid and the Nafamostat showed an average number of intermolecular hydrogen bonds of 1.196803197 ± 0.937139141, 1.545454545 ± 1.018912076, 0.754245754 ± 0.907493502 and 1.632367632 ± 1.051052467 respectively which aids in the stabilization of the protein–ligand complexes (Fig. S1.B).

The binding free energies from MD simulation studies were found to be negative for Apigenin (ΔPB = -12.37 kcal/mol, ΔGB = -12.37 kcal/mol), Luteolin (ΔPB = -6.40 kcal/mol, ΔGB = -10.05 kcal/mol), Ferulic acid (ΔPB = -2.40 kcal/mol, ΔGB = -0.24 kcal/mol) and Nafamostat (ΔPB = -9.30 kcal/mol, ΔGB = -24.91 kc al/mol) (Table S2). The van der Waals energy make a significant

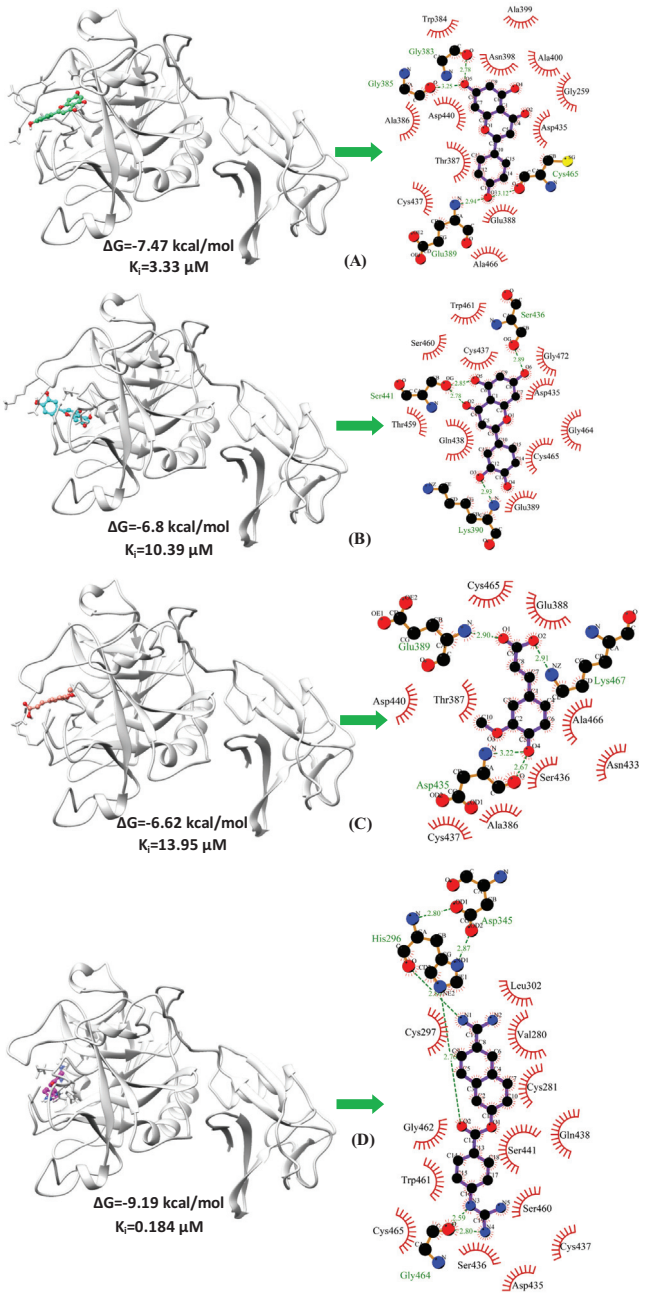

Fig. 3. The binding conformation and molecular interactions of the compounds-(A) Apigenin (B) Luteolin (C) Ferulic acid and (D) Nafamostat with the target receptor TMPRSS2. On the left panel, the drug-receptor is depicted as a grey ribbon and compounds-Apigenin (spring green), Luteolin (cyan), Ferulic acid (salmon) and Nafamostat (magenta) are shown in ball and stick representations. On the right panel are displayed the molecular interactions between the compounds and the receptor with the hydrogen bonds shown in green and hydrophobic interactions shown in red semi-arcs.

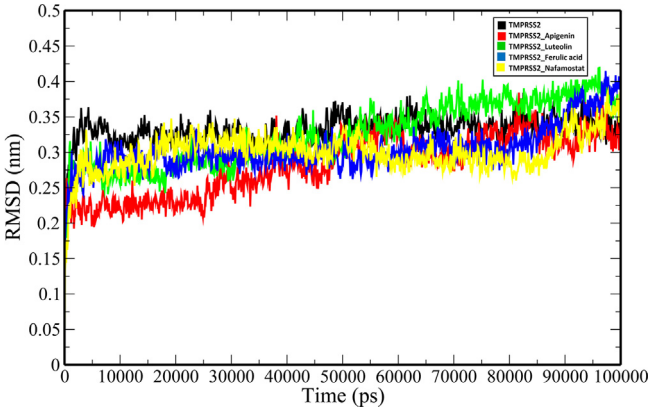

Fig. 4. RMSD plot of unbound TMPRSS2 (black) and docked TMPRSS2 backbone atoms (TMPRSS2_Apigenin: red; TMPRSS2_Luteolin: green; TMPRSS2_Ferulic acid: blue and TMPRSS2_Nafamostat).

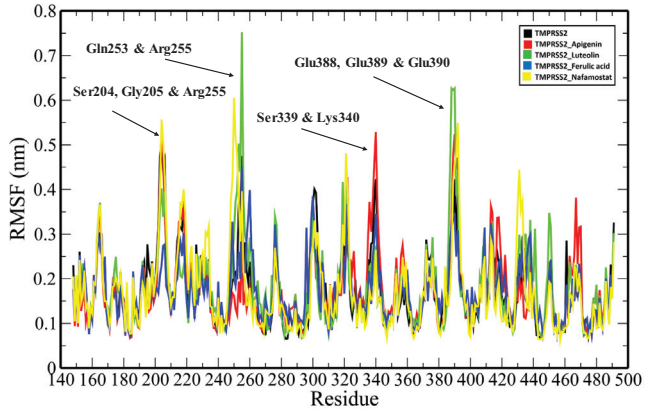

Fig. 5. RMSF plot of unbound TMPRSS2 (black) and TMPRSS2 docked complexes (TMPRSS2_Apigenin: red; TMPRSS2_Luteolin: green; TMPRSS2_Ferulic acid: blue and TMPRSS2_Nafamostat) where residues with large amplitude of fluctuations are marked and labelled.

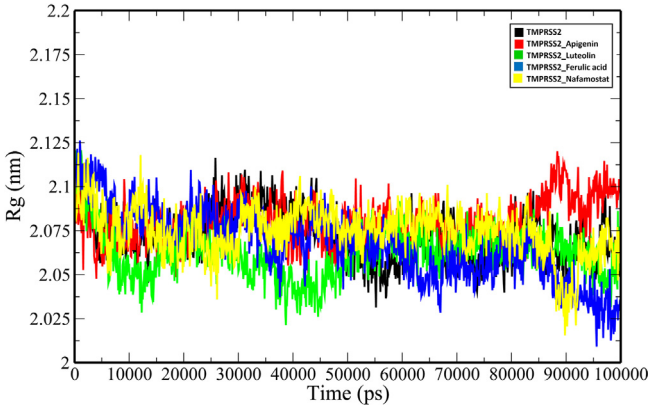

Fig. 6. Rg plot of unbound TMPRSS2 and TMPRSS2 docked complexes (TMPRSS2_Apigenin: red; TMPRSS2_Luteolin: green; TMPRSS2_Ferulic acid: blue and TMPRSS2_Nafamostat).

contribution to the binding free energy except for Ferulic acid where the electrostatic energy component has predominant contributions. The key residues contributing towards the binding interaction between Apigenin and TMPRSS2 include Gly259 (−1.25 kcal/mol), Cys437 (−1.22 kcal/mol), Asn398 (−1.06 kcal/mol), Ala466 (−1.01 kcal/mol), Val434 (−0.95 kcal/mol), Ala399 (−0.82 kcal/mol), Asp435 (−0.80 kcal/mol), Thr387 (−0.74 kcal/mol), Ile381 (−0.68 kcal/mol) and Ala400 (−0.54 kcal/mol) (Fig. S2.A). In case of TMPRSS2_Luteolin complex, residues such as Cys465 (−1.69 kcal/mol), Gln438 (−1.47 kcal/mol), Cys437 (−1.04 kcal/mol), Gly462 (−0.96 kcal/mol), Gly464 (−0.96 kcal/mol), Glu389 (−0.91 kcal/mol), Trp461 (−0.78 kcal/mol), Lys390 (−0.75 kcal/mol), Ser436 (−0.63 kcal/mol), Thr459 (−0.58 kcal/mol) contribute majorly to the total binding energy (Fig. S2.B). The top ten residues contributing towards the

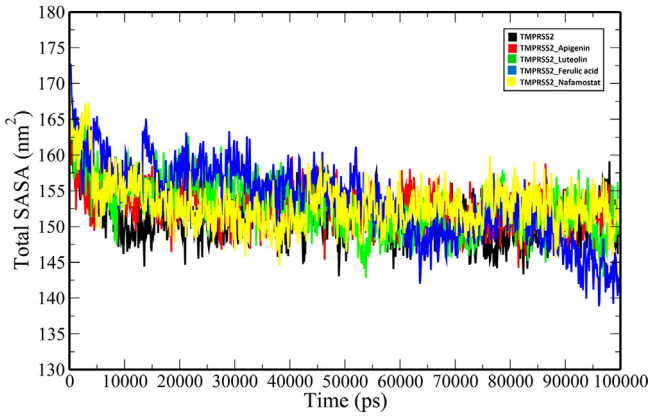

Fig. 7. Total SASA plot of unbound TMPRSS2 and TMPRSS2 docked complexes (TMPRSS2_Apigenin: red; TMPRSS2_Luteolin: green; TMPRSS2_Ferulic acid: blue and TMPRSS2_Nafamostat).

binding interaction between Ferulic acid and TMPRSS2 include Lys401 (−1.40 kcal/mol), Leu378 (−1.26 kcal/mol), Leu403 (−0.65 kcal/mol), Phe429 (−0.47 kcal/mol), Val402 (−0.17 kcal/mol), Arg252 (−0.07 kcal/mol), Trp380 (−0.06 kcal/mol), Lys449 (−0.06 kcal/mol), Arg255 (−0.05 kcal/mol) and Arg409 (−0.05 kcal/mol) (Fig. S2.C). In case of TMPRSS2_Nafamostat complex, residues such as Gln438 (−2.00 kcal/mol), Cys437 (−1.37 kcal/mol), Asp435 (−1.33 kcal/mol), Trp461 (−1.32 kcal/mol), Pro471 (−1.15 kcal/mol), Gly472 (−0.89 kcal/mol), Gly462 (−0.85 kcal/mol), Cys465 (−0.79 kcal/mol), Leu430 (−0.72 kcal/mol) and Gly432 (−0.68 kcal/mol) have higher contribution toward the total binding energy (Fig. S2.D).

4. Discussion

The SARS-CoV-2, the causative agent of COVID-19 depends on the host multi-domain type II transmembrane serine protease, transmembrane protease serine 2 (TMPRSS2) angiotensin-converting enzyme 2 (ACE2) receptor for the cleavage process of S proteins to enter the host cells. *Platycodon grandiflorus* (Jacq.) A. DC. which belongs to the Campanulaceae family has immense medicinal importance. The rhizomes of *P. grandiflorus* have not only been widely utilized in traditional Chinese medicine (TCM) but also has been traditionally used in various Japanese prescriptions. More recently, Kim et al. (2021) found that platycodin D (PD), a triterpenoid saponin rich in *P. grandiflorus* efficiently prevents SARS-CoV-2 infection via lysosome and transmembrane protease serine 2 (TMPRSS2)-driven entry. Therefore, the bioactive phytochemicals of *P. grandiflorus* can be explored as a source of novel chemical entities to block the replication of SARS-CoV-2. Given the importance of TMPRSS2 in viral entry and the dearth of effective therapeutics for the present COVID-19 pandemic, small compounds or the Food and Drug Administration (FDA)-approved drugs can be tested for their ability to suppress the enzyme's activity. Camostat, nafamostat, and gabexate which are clinically authorized pharmacologic treatments of pancreatitis in Japan have been also used to suppress the activity of TMPRSS2 (Yamaya et al., 2020) and these known inhibitors have IC_{50} values of 6.2 nM, 0.27 nM and 130 nM respectively (Shrimp et al., 2020). A recent study suggested that nafamostat was protective against SARS-CoV-2 pulmonary infections in two mouse models for COVID-19 (Li et al., 2021). Given the relevance of host TMPRSS2 in the pathogenesis of SARS-CoV-2 infections, our present research focuses on identifying active *Platycodon grandiflorus* compounds as potential TMPRSS2 inhibitors, which would then prevent SARS-CoV-2 from infecting host cells. We have used a diverse set of 34 phytochemicals of *P. grandiflorus* and applied drug filters to assess their oral bioavailability. The ability of the filtered drug-like compounds to bind and interact with the target receptor TMPRSS2 was investigated. The best three molecules interacting with the drug-receptor TMPRSS2 identified were Apigenin, Luteolin and Ferulic acid which bind to the active pocket with hydrogen bonds and hydrophobic interactions. 100 ns MD simulations were performed to evaluate the dynamic behaviour of the protein–ligand complexes and their stabilities were assessed in terms of RMSD, Rg, SASA and number of hydrogen bonds. Apigenin (4′,5,7-trihydroxy flavone), a flavone family member, is a dietary flavonoid that is both nontoxic and nonmutagenic and it has hydroxyl groups in both its B and C rings (Wang et al., 2020). Apigenin has antiviral properties *in vitro* and *in vivo* against a variety of viruses, including enterovirus 71 (EV71) (Lv et al., 2014; Zhang et al., 2014), hepatitis C virus (HCV) (Ahmed-Belkacem et al., 2014), Human Immunodeficiency Virus (HIV) (Kehinde et al., 2019), and adenoviruses (Kanerva et al., 2007). Apigenin inhibited HCV replication by lowering the levels of mature miR122 expression (Shibata et al., 2014) and suppressed FMDV (Foot and Mouth Disease Virus) infection at the post-entry stage by reducing internal ribosome entry site (IRES)-driven translational activity (Qian et al., 2015). Epstein-Barr virus (EBV) reactivation into the lytic cycle and virion generation by EBV-positive nasopharyngeal carcinoma (NPC) cells are both inhibited by apigenin (Wu et al., 2017). Luteolin (3,4,5,7-tetrahydroxyflavone) is a clear yellow crystal that belongs to the bioflavonoid family (Wang et al., 2020). By blocking the host proprotein convertase furin, luteolin can obstruct the later stages of the dengue virus (DENV) viral life cycle in infected cells (Peng et al., 2017), Epstein-Barr virus (Wu et al., 2016), Japanese encephalitis virus (Fan et al., 2016), HIV-1 (Mehla et al., 2011), Hepatitis B virus (Bai et al., 2016) and influenza A virus (Yan et al., 2019) are all inhibited by luteolin. The previous study suggests that the flavonoids-Apigenin and Luteolin inhibit SARS-CoV $3CL^{pro}$ activity as well with IC_{50} values of 280.8 μM and 20.2 μM respectively (Ryu et al., 2010). Besides, luteolin has been found to block the entry of SARS-CoV (EC_{50} = 10.6 μM) into host cells by binding to the surface spike protein (Yi et al., 2004). While our findings are encouraging, additional *in vitro* or *in vivo* studies are needed to determine the anti-SARS-CoV-2 efficacy of the compounds. Further, in TMPRSS2cells, severe acute respiratory syndrome coronavirus 2 (SARS-CoV) S can use the endosomal cysteine proteases cathepsin B and L (CatB/L) for S protein priming (Simmons et al., 2005) and therefore it would be fascinating to see if these compounds have similar inhibitory activity against them. Because TMPRSS2 functions as a viral protein processing protease in the pathogenesis of other coronaviruses-SARS-CoV, Middle East respiratory syndrome coronavirus (MERS-CoV), as well as influenza viruses (Mahoney et al., 2021), these lead compounds may be quite promising to be developed as broad-spectrum antivirals. The compounds could be subjected to structure–activity studies in order to enhance their potency and specificity.

5. Conclusion

The paucity of effective therapeutic medications for SARS-CoV-2 infections, as well as the rising mortality rate, necessitate the development of innovative drug candidate molecules with few adverse effects. Here, we explored the bioactive phytochemicals from a traditionally important medicinal plant *Platycodon grandiflorus* as a source of novel molecules for the inhibition of cellular TMPRSS2 activity, a key pharmacological target for preventing the SARS-CoV-2 entry into the host cells. Our study concludes that Apigenin, Luteolin and Ferulic acid are the most effective com-

pounds for inhibition of the TMPRSS2 activity demonstrating that these agents may be used in COVID-19 treatment. These compounds should be subjected to further experimental studies to confirm their efficacies.

Declaration of Competing Interest

The authors declare that they have no known competing financial interests or personal relationships that could have appeared to influence the work reported in this paper.

Acknowledgements

The authors would like to extend their sincere appreciation to the Researchers Supporting Project number (RSP2022R418), King Saud University, Riyadh, Saudi Arabia.

Appendix A. Supplementary data

Supplementary data to this article can be found online at https://doi.org/10.1016/j.jksus.2022.102155.

References

Ahmed-Belkacem, A., Guichou, J.-F., Brillet, R., Ahnou, N., Hernandez, E., Pallier, C., Pawlotsky, J.-M., 2014. Inhibition of RNA binding to hepatitis C virus RNA-dependent RNA polymerase: a new mechanism for antiviral intervention. Nucleic Acids Res. 42 (14), 9399–9409.

Bai, L., Nong, Y., Shi, Y., Liu, M., Yan, L., Shang, J., Huang, F., Lin, Y., Tang, H., 2016. Luteolin inhibits hepatitis B virus replication through extracellular signal-regulated kinase-mediated down-regulation of hepatocyte nuclear factor 4$¤$ expression. Mol. Pharm. 13 (2), 568–577.

Baughn, L.B., Sharma, N., Elhaik, E., Sekulic, A., Bryce, A.H., Fonseca, R., 2020. Targeting TMPRSS2 in SARS-CoV-2 infection. Mayo Clinic Proceed. 95 (9), 1989–1999.

Bavi, R., Kumar, R., Rampogu, S., Son, M., Park, C., Baek, A., Kim, H.-H., Suh, J.-K., Park, S.J., Lee, K.W., 2016. Molecular interactions of UvrB protein and DNA from Helicobacter pylori: Insight into a molecular modeling approach. Comput. Biol. Med. 75, 181–189.

Berendsen, H.J.C., Postma, J.P.M., van Gunsteren, W.F., DiNola, A., Haak, J.R., 1984. Molecular dynamics with coupling to an external bath. J. Chem. Phys. 81 (8), 3684–3690.

China Pharmacopoeia Committee, 2005 China Pharmacopoeia Committee, (Eds.), 2005. Pharmacopoeia of the People's Republic of China, the first division of 2005 edition. China Chemical Industry Press, Beijing, pp. 291–292.

Darden, T., York, D., Pedersen, L., 1993. Particle mesh Ewald: An N· log (N) method for Ewald sums in large systems. J. Chem. Phys. 98 (12), 10089–10092.

Fan, W., Qian, S., Qian, P., Li, X., 2016. Antiviral activity of luteolin against Japanese encephalitis virus. Virus Res. 220, 112–116.

Fathema, K., Hassan, M.N., Mazumder, M.W., Benzamin, M., Ahmed, M., Islam, M.R., Haque, N., Sutradhar, P.K., Rahman, A.R., Rukunuzzaman, M., 2021. COVID 19 in children: gastrointestinal, hepatobiliary and pancreatic manifestation. Mymensingh Med. J. MMJ 30, 570–579.

Fuentes-Prior, P., 2021. Priming of SARS-CoV-2 S protein by several membrane-bound serine proteinases could explain enhanced viral infectivity and systemic COVID-19 infection. J. Biol. Chem., 296

Gemmati, D., Bramanti, B., Serino, M.L., Secchiero, P., Zauli, G., Tisato, V., 2020. COVID-19 and individual genetic susceptibility/receptivity: role of ACE1/ACE2 genes, immunity, inflammation and coagulation. Might the double X-chromosome in females be protective against SARS-CoV-2 compared to the single X-chromosome in males? Int. J. Mol. Sci. 21, 3474.

Halgren, T.A., 1996. Merck molecular force field. I. Basis, form, scope, parameterization, and performance of MMFF94. J. Comput. Chem. 17, 490–519. https://doi.org/10.1002/(SICI)1096-987X(199604)17:5/6<490::AID-JCC1>3.0.CO;2-P.

Hao, G.-F., Zhu, X.-L., Ji, F.-Q., Zhang, L., Yang, G.-F., Zhan, C.-G., 2009. Understanding the mechanism of drug resistance due to a codon deletion in protoporphyrinogen oxidase through computational modeling. J. Phys. Chem. B 113 (14), 4865–4875.

Hess, B., Kutzner, C., Van Der Spoel, D., Lindahl, E., 2008. GRGMACS 4: Algorithms for highly efficient, load-balanced, and scalable molecular simulation. J. Chem. Theory Comput. 4, 435–447. https://doi.org/10.1021/ct700301q.

Hoffmann, M., Kleine-Weber, H., Schroeder, S., Krüger, N., Herrler, T., Erichsen, S., Schiergens, T.S., Herrler, G., Wu, N.-H., Nitsche, A., Müller, M.A., Drosten, C., Pöhlmann, S., 2020. SARS-CoV-2 cell entry depends on ACE2 and TMPRSS2 and is blocked by a clinically proven protease inhibitor. Cell 181 (2), 271–280.e8.

Hou, T., Wang, J., Li, Y., Wang, W., 2011. Assessing the performance of the MM/PBSA and MM/GBSA methods. 1. The accuracy of binding free energy calculations based on molecular dynamics simulations. J. Chem. Inf. Model. 51 (1), 69–82.

Huang, P.H., 2008. Flora of China. Science Press, Beijing.

Kanerva, A., Raki, M., Ranki, T., Särkioja, M., Koponen, J., Desmond, R.A., Helin, A., Stenman, U.-H., Isoniemi, H., Höckerstedt, K., Ristimäki, A., Hemminki, A., 2007. Chlorpromazine and apigenin reduce adenovirus replication and decrease replication associated toxicity. J. Gene Med. A cross-disciplinary. J. Res. Sci. gene Transf. Clin. Appl. 9 (1), 3–9.

Kaur, U., Chakrabarti, S.S., Ojha, B., Pathak, B.K., Singh, A., Saso, L., Chakrabarti, S., 2021. Targeting host cell proteases to prevent SARS-CoV-2 invasion. Curr. Drug Targets 22 (2), 192–201.

Kehinde, I., Ramharack, P., Nlooto, M., Gordon, M., 2019. The pharmacokinetic properties of HIV-1 protease inhibitors: A computational perspective on herbal phytochemicals. Heliyon 5, (10) e02565.

Kim, S., Thiessen, P.A., Bolton, E.E., Chen, J., Fu, G., Gindulyte, A., Han, L., He, J., He, S., Shoemaker, B.A., Wang, J., Yu, B., Zhang, J., Bryant, S.H., 2016. PubChem substance and compound databases. Nucleic Acids Res 44 (D1), D1202–D1203.

Kim, T.Y., Jeon, S., Jang, Y., Gotina, L., Won, J., Ju, Y.H., Kim, S., Jang, M.W., Won, W., Park, M.G., Pae, A.N., Han, S., Kim, S., Lee, C.J., 2021. Platycodin D, a natural component of Platycodon grandiflorum, prevents both lysosome-and TMPRSS2-driven SARS-CoV-2 infection by hindering membrane fusion. Exp. Mol. Med. 53 (5), 956–972.

Laskowski, R.A., Swindells, M.B., 2011. LigPlot+: multiple ligand-protein interaction diagrams for drug discovery. J. Chem. Inf. Model. 51, 2778–2786. https://doi.org/10.1021/ci200227u.

Lee, E.B., 1973. Pharmacological studies on Platycodon grandiflorum A. DC. IV. A comparison of experimental pharmacological effects of crude platycodin with clinical indications of platycodi radix (author's transl). Yakugaku zasshi J. Pharm. Soc. Japan 93 (9), 1188–1194.

Li, K., Meyerholz, D.K., Bartlett, J.A., McCray, P.B., Frieman, M.B., Griffin, D.E., 2021. The tmprss2 inhibitor nafamostat reduces sars-cov-2 pulmonary infection in mouse models of covid-19. MBio 12, (4) e00970-21.

Lipinski, C.A., 2004. Lead- and drug-like compounds: the rule-of-five revolution. Drug Discov. Today. Technol. 1, 337–341. https://doi.org/10.1016/j.ddtec.2004.11.007.

Lv, X., Qiu, M., Chen, D., Zheng, N., Jin, Y., Wu, Z., 2014. Apigenin inhibits enterovirus 71 replication through suppressing viral IRES activity and modulating cellular JNK pathway. Antiviral Res. 109, 30–41.

Mahoney, M., Damalanka, V.C., Tartell, M., Chung, D.H., Lourenco, A.L., Pwee, D., Bridwell, A.E.M., Hoffmann, M., Voss, J., Karmakar, P., others, 2021. A novel class of TMPRSS2 inhibitors potently block SARS-CoV-2 and MERS-CoV viral entry and protect human epithelial lung cells. bioRxiv.

Matsuyama, S., Nao, N., Shirato, K., Kawase, M., Saito, S., Takayama, I., Nagata, N., Sekizuka, T., Katoh, H., Kato, F., Sakata, M., Tahara, M., Kutsuna, S., Ohmagari, N., Kuroda, M., Suzuki, T., Kageyama, T., Takeda, M., 2020. Enhanced isolation of SARS-CoV-2 by TMPRSS2-expressing cells. Proc. Natl. Acad. Sci. 117 (13), 7001–7003.

Mehla, R., Bivalkar-Mehla, S., Chauhan, A., Vij, N., 2011. A flavonoid, luteolin, cripples HIV-1 by abrogation of tat function. PLoS One 6, (11) e27915.

Morris, G.M., Goodsell, D.S., Halliday, R.S., Huey, R., Hart, W.E., Belew, R.K., Olson, A.J., 1998. Automated docking using a Lamarckian genetic algorithm and an empirical binding free energy function. J. Comput. Chem. 19 (14), 1639–1662.

Morris, G.M., Huey, R., Lindstrom, W., Sanner, M.F., Belew, R.K., Goodsell, D.S., Olson, A.J., 2009. AutoDock4 and AutoDockTools4: Automated docking with selective receptor flexibility. J. Comput. Chem. 30, 2785–2791. https://doi.org/10.1002/jcc.21256.

Pan, Y., Gao, D., Zhan, C.-G., 2008. Modeling the catalysis of anti-cocaine catalytic antibody: competing reaction pathways and free energy barriers. J. Am. Chem. Soc. 130 (15), 5140–5149.

Parrinello, M., Rahman, A., 1981. Polymorphic transitions in single crystals: A new molecular dynamics method. J. Appl. Phys. 52 (12), 7182–7190.

Peng, M., Watanabe, S., Chan, K.W.K., He, Q., Zhao, Y., Zhang, Z., Lai, X., Luo, D., Vasudevan, S.G., Li, G., 2017. Luteolin restricts dengue virus replication through inhibition of the proprotein convertase furin. Antiviral Res. 143, 176–185.

Qian, S., Fan, W., Qian, P., Zhang, D., Wei, Y., Chen, H., Li, X., 2015. Apigenin restricts FMDV infection and inhibits viral IRES driven translational activity. Viruses 7, 1613–1626.

Ryu, Y.B., Jeong, H.J., Kim, J.H., Kim, Y.M., Park, J.-Y., Kim, D., Naguyen, T.T.H., Park, S.-J., Chang, J.S., Park, K.H., et al., 2010. Biflavonoids from Torreya nucifera displaying SARS-CoV 3CLpro inhibition. Bioorg. Med Chem. 18, 7940–7947.

Sander, T., Freyss, J., von Korff, M., Rufener, C., 2015. DataWarrior: an open-source program for chemistry aware data visualization and analysis. J. Chem. Inf. Model. 55, 460–473. https://doi.org/10.1021/ci500588j.

Schüttelkopf, A.W., van Aalten, D.M.F., 2004. PRODRG: a tool for high-throughput crystallography of protein–ligand complexes. Acta Crystallogr. Sect. D Biol. Crystallogr. 60 (8), 1355–1363.

Shibata, C., Ohno, M., Otsuka, M., Kishikawa, T., Goto, K., Muroyama, R., Kato, N., Yoshikawa, T., Takata, A., Koike, K., 2014. The flavonoid apigenin inhibits hepatitis C virus replication by decreasing mature microRNA122 levels. Virology 462, 42–48.

Shrimp, J.H., Kales, S.C., Sanderson, P.E., Simeonov, A., Shen, M., Hall, M.D., 2020. An enzymatic TMPRSS2 assay for assessment of clinical candidates and discovery of inhibitors as potential treatment of COVID-19. ACS Pharmacol. Transl. Sci. 3, 997–1007.

Simmons, G., Gosalia, D.N., Rennekamp, A.J., Reeves, J.D., Diamond, S.L., Bates, P., 2005. Inhibitors of cathepsin L prevent severe acute respiratory syndrome coronavirus entry. Proc. Natl. Acad. Sci. 102 (33), 11876–11881.

Takagi, K., Lee, E.B., 1972. Pharmacological studies on Platycodon grandiflorum A. DC. 3. Activities of crude platycodin on respiratory and circulatory systems and its other pharmacological activities. Yakugaku zasshi J. Pharm. Soc. Japan 92, 969–973.

Wang, L., Song, J., Liu, A., Xiao, B., Li, S., Wen, Z., Lu, Y., Du, G., 2020. Research progress of the antiviral bioactivities of natural flavonoids. Nat. Products Bioprospect. 10 (5), 271–283.

Wu, C.-C., Fang, C.-Y., Cheng, Y.-J., Hsu, H.-Y., Chou, S.-P., Huang, S.-Y., Tsai, C.-H., Chen, J.-Y., 2017. Inhibition of Epstein-Barr virus reactivation by the flavonoid apigenin. J. Biomed. Sci. 24, 1–13.

Wu, C.-C., Fang, C.-Y., Hsu, H.-Y., Chen, Y.-J., Chou, S.-P., Huang, S.-Y., Cheng, Y.-J., Lin, S.-F., Chang, Y., Tsai, C.-H., Chen, J.-Y., 2016. Luteolin inhibits Epstein-Barr virus lytic reactivation by repressing the promoter activities of immediate-early genes. Antiviral Res. 132, 99–110.

Yamaya, M., Nishimura, H., Deng, X., Kikuchi, A., Nagatomi, R., 2020. Protease inhibitors: candidate drugs to inhibit severe acute respiratory syndrome coronavirus 2 replication. Tohoku J. Exp. Med. 251 (1), 27–30.

Yan, H., Ma, L., Wang, H., Wu, S., Huang, H., Gu, Z., Jiang, J., Li, Y., 2019. Luteolin decreases the yield of influenza A virus in vitro by interfering with the coat protein I complex expression. J. Nat. Med. 73 (3), 487–496.

Yang, J.-F., Wang, F., Chen, Y.-Z., Hao, G.-F., Yang, G.-F., 2020. LARMD: integration of bioinformatic resources to profile ligand-driven protein dynamics with a case on the activation of estrogen receptor. Brief. Bioinform. 21, 2206–2218.

Yi, L., Li, Z., Yuan, K., Qu, X., Chen, J., Wang, G., Zhang, H., Luo, H., Zhu, L., Jiang, P., Chen, L., Shen, Y., Luo, M., Zuo, G., Hu, J., Duan, D., Nie, Y., Shi, X., Wang, W., Han, Y., Li, T., Liu, Y., Ding, M., Deng, H., Xu, X., 2004. Small molecules blocking the entry of severe acute respiratory syndrome coronavirus into host cells. J. Virol. 78 (20), 11334–11339.

Zhang, L., Wang, Y., Yang, D., Zhang, C., Zhang, N., Li, M., Liu, Y., 2015. Platycodon grandiflorus–An Ethnopharmacological, phytochemical and pharmacological review. J. Ethnopharmacol. 164, 147–161.

Zhang, W., Qiao, H., Lv, Y., Wang, J., Chen, X., Hou, Y., Tan, R., Li, E., Qiu, J., 2014. Apigenin inhibits enterovirus-71 infection by disrupting viral RNA association with trans-acting factors. PLoS One 9 (10). e110429.